COMPARISON BETWEEN DINSAR AND STACKING IN DEFORMATION MONITORING USING LUTAN-1

Jing Lu[1], Xinming Tang[1], Tao Li[1], Xiang Zhang[1], Xuefei Zhang[1], Tan Li[2], Xiaofeng Qiu[2]

[1]*Land Satellite Remote Sensing Application Center, MNR, Beijing 100048, China*
[2] *Beijing SatImage Information Technology Co.,Ltd., Beijing 100040, China*

KEY WORDS: LANDSAR, LT-1, DINSAR, STACKING, DEFORMATION MONITORING

ABSTRACT:

LuTan-1 (LT-1) satellite constellation is used to conduct surface deformation monitoring. Following the successful launch of two satellites, we began to use the independently developed LandSAR software for differential interferometric data processing and application at the beginning of 2022. In this paper, we tested the LandSAR software by assessing the DInSAR and stacking modules. We used 21 LT-1 single look complex (SLC) images from December 2022 to May 2023 to conduct DInSAR and stacking processing of Datong City, Shanxi Province. DInSAR revealed more subsidence funnels and larger relative deformation values compared to stacking. We tested the DInSAR technology with different parameter combination. Results show that multi-looking factor is the most important to detect the deformation details because of the phase gradient limitation of DInSAR. Compared multi-looking ratios of 2×2 and 4×4, the subsiding funnels that were detected decreased from 60 to 47. After deep testing and assessment, we found that the linear model used by stacking affects the result severely, meaning that most of the subsidence of coal mines were not linear. Stacking only found 32 subsidence funnels which were active coal mines during our observation time. The test result show that LandSAR was compatible for DInSAR and stacking. And it is useful to observe linear and nonlinear deformation in the coal mine regions.

1. INTRODUCTION

Space-borne interferometric synthetic aperture radar (InSAR) is an important tool for surface deformation research developed in recent years. China's LuTan-1 (LT-1) satellite constellation focuses on surface deformation monitoring (Li et al., 2022). Following the successful launch of two satellites, we began to use the independently developed LandSAR software for differential interferometric data processing and application at the beginning of 2022. LandSAR software was designed initially for Chinese differential InSAR satellite constellation applications (Lu et al.2023). Now it supports nearly all the commonly used SAR satellites including TerraSAR-X/TanDEM-X, Cosmo-SkyMed, ALOS-PALSAR, and RadarSat etc. It also supports the typical interferometric applications such as digital surface model (DSM) generation and deformation monitoring (Li et al., 2019).

We have defined three kinds of deformation products. They are deformation field product generated using Differential InSAR (DInSAR), deformation velocity field product generated using stacking, and multi-temporal deformation product generated using MT-InSAR. LandSAR supports the operational processing of DInSAR. We have introduced the DEM of ZY-3 and Copernicus, as well as precise orbit data to ensure product quality. Now we can process an average of 800 scenes of LT-1 satellite data each day. Besides, we estimate the baseline and remove the baseline-terrain related error. The phase ramp related to the perpendicular baseline is also modelled and removed using LandSAR. However, we still found that DInSAR is affected by various types of error sources such as baseline error, atmospheric error, and terrain residual error. Stacking and multi-temporal InSAR(MTInSAR) methods are developed and is now being tested to remove the residual error and provide reliable results (Li et al., 2023; Lu et al., 2023).

LandSAR support stacking analysis using more than 10 images (Xu et al., 2022a). Based on the assumption that the ground deformation presents a linear change, atmospheric delay and the other phase random errors are suppressed by the weighted average processing of the interferometric pairs, so as to realize the accurate extraction of the ground deformation velocity field. LandSAR supports the superimposition processing of linear deformation and the optimization analysis of deformation rate. To further remove the residual error, we introduced a refinement method in the step of deformation rate calculating.

2. DATA AND METHODS

2.1 Study area and data introduction

The revisit period of LT-1 satellites is 8 days for single satellite and 4 days for double satellites, and the orbital tube radius is 350 meters. LT-1 satellites mainly use strip mode 1 and strip mode 2 to carry out deformation monitoring tasks. The resolutions are 3 meters and 12 meters respectively, and the swath widths are 50 kilometres and 100 kilometres respectively. From before April of 2023, we observed the deformation mainly used strip mode 2. At

some areas of interest (AOI), we collected the data every 4 days, more than 20 images have been provided during in-orbit test time. The data are useful to carry out large-scale and long-term subsidence monitoring.

Datong coalfield is one of the eight major coal production bases in China, located in the southwest of Datong City, belonging to the Yungang region. Long-term large-scale mining has caused serious surface deformation in Datong coalfield, resulting in ground subsidence, collapse and other problems, involving a wide range of areas, bringing a series of social and environmental problems to the surrounding areas of the mining area. In addition, the terrain in this area is mostly undulating mountains and hilly areas, with abundant data accumulation and sparse vegetation, making it an ideal research area. Table 1 gives detailed parameters of the selected Datong coalfield data of LT-1. In this study, we used the 21 cropped LT-1 satellite data from December 2022 to May 2023 to conduct DInSAR and stacking processing using LandSAR, comparing and analysing the results of the two methods.

Date(YYYYMMDD)	
20221215	20230329
20230116	20230402
20230128	20230406
20230124	20230410
20230201	20230414
20230209	20230418
20230217	20230508
20230225	20230512
20230305	20230516
20230313	20230520
20230321	

Table 1. Date of the chosen Datong data

2.2 Methods

Firstly, we selected 21 LT-1 satellite data from December 2022 to May 2023. Unlike GAMMA and other InSAR processing softwares, LandSAR supports image crop before co-registration. About 100 pixel of the borders are extended to ensure the full coverage of the AOI. The function is especially designed to decrease the time consumed. After that, LandSAR carries out DInSAR processing containing co-registration, resampling, generating interferograms, flattening, filtering, phase unwrapping, baseline refinement, phase restoring and fitting, phase-deformation conversion, geocoding, and quality assessment (Gao et al., 2019; Gao et al., 2020). Stacking processing of LandSAR includes temporal registration, common region cropping, interferometric pairs selecting, DInSAR processing, and deformation rate calculating (Johnsen et al., 2007; Xiang et al., 2018).

Secondly, we selected two images with baseline coherence of 0.97 from the 21 scenes to conduct DInSAR processing flow using LandSAR (Molan et al., 2018). We tested the DInSAR technology with different parameter combination. Results show that multi-looking factor is the most important to detect the deformation details because of the phase gradient limitation of DInSAR. We compared multi-looking ratios of 2×2 and 4×4 in both range and azimuth direction with other parameters unchanged.

Finally, we conducted stacking processing using all 21 scenes. In order to ensure processing accuracy, we selected the post-stacking option to refine the results. The post-processing will determine whether the pixels meet the linear deformation requirements and perform a coherence threshold processing (Frascatti， 2003). After deep testing and assessment, we found that the linear model used by stacking affects the result severely, deformation before and after linear model refinement have been analysed in our paper.

3. RESULTS AND ANALYSIS

3.1 Analysis of DInSAR results

The result with a 4×4 multi-looking factor presents 47 subsidence areas. According to the coherence map, we found that the mean value of coherence is 0.986, standard deviation is 0.088, and 87.65% of the points have a coherence of over 0.99, as shown in Fig. 1(a) (Zhang et al., 2021). However, we found that many deformation fields have experienced de-coherent in their central subsiding funnels. This is induced by the large phase gradient affected by the large multi-looking factor. To improve the de-coherent phenomenon, we used LandSAR for processing with smaller multi-looking factor. We found that the number of subsidence areas increased to 60 in the result with a 2×2 multi-look factor. But as the multi-looking factors decrease from 4×4 to 2×2, the coherence decreases slightly, as shown in Fig.1. Compared with the results using a 4×4 multi-look factor, it can be seen from Fig. 1(b) that the results using a 2×2 multi-look factor have significantly lower coherence due to increased noise. The mean value of coherence is 0.98, standard deviation drops to 0.079, and only 63.7% of the points have coherence above 0.99. However, due to the decrease in phase gradient, as the multi-look factor decreases, the number of empty values in the deformation field decreases, as shown in Fig. 2 and Fig.3.

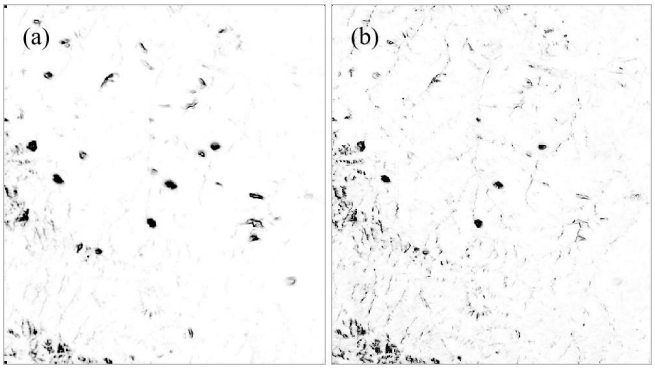

Figure 1. DInSAR coherent maps with the multi-look factor of 4×4 and 2×2, (a) is the coherent map with 4×4 multi-look factor, (b) is the coherent map with 2×2 multi-look factor.

Fig.2 and Fig.3 indicate the deformation results with 2×2 and 4×4 multi-look factor of the study area. The deformation amounts range from -0.15 to 0.04 meters. We circle six regions from (a) to (f) in the two results for comparative analysis. Area (a) appears to be a subsidence funnel in Fig. 2, but in Fig. 3 it becomes ambiguous. From areas (b), (c), (e), and (f), the null value areas decreased with

the 2×2 multi-look factor, while which becomes more with a higher multi-look factor due to the increase of phase gradient. At the same time, there is a lot of speckle noise in area (d) when the multi-look factor is lower, while the residuals in the same region are greatly eliminated after increasing the multi-look factor to 4×4.

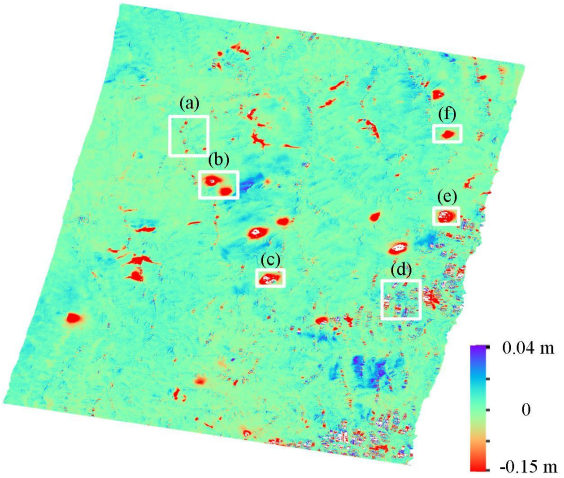

Figure 2. The deformation results with 2×2 multi-look factor. (a) is a suspected deformation field. (b), (c), (e) and (f) are typical subsidence areas. (d) indicates the noise elimination.

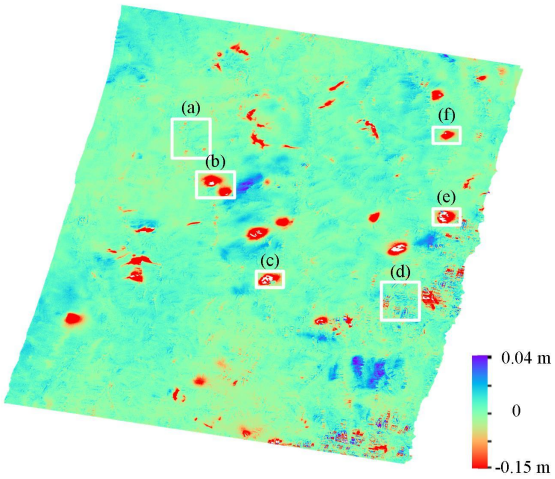

Figure 3. The deformation results with 4×4 multi-look factor. (a) is a suspected deformation field. (b), (c), (e) and (f) are typical subsidence areas. (d) shows the noise elimination.

3.2 Analysis of stacking results

The processing accuracy of stacking is higher than that of conventional DInSAR, which can better remove residuals. Although the results of stacking can greatly reduce the residual error, this method cannot remove all the noise, so we added a refinement method to eliminate the points of nonlinear deformation in the deformation rate calculation step (Zhang et al., 2021).

After refinement, the subsidence velocity values vary from -1.48 to 0.18. It can be seen from Fig. 4(b) that there is almost no obvious residual in the refined image. However, the main deformation fields of stacking velocity results basically showed a lot of de-coherence. Before refinement, the subsidence velocity values vary from -2.18 to 0.26 m/a, see Fig. 4(a). The deformation field no longer has obvious null values, indicating that the deformation data in the region is continuous and complete, with no missing or abnormal cases. After comparison, it can be found that the range of the refined deformation rate value has been narrowed. The comparison of images before and after refining can be inferred that the deformation of the coal mine does not fully comply with the linear deformation law (Zhang et al., 2013).

Non-linear deformation may be caused by the combined action of various factors, including mining activities, geological tectonic movements, and changes in groundwater pressure (Zhu et al., 2015). For example, the disturbance and destruction of strata during mining processes may lead to non-linear subsidence or uplift of the surface; geological tectonic movements may cause folds, fractures, and other phenomena in the strata; changes in groundwater pressure may cause bulging or depression of the surface. Non-linear deformation may lead to geological disasters such as ground collapse and slope instability, and may also damage infrastructure such as buildings and roads within the mining area.

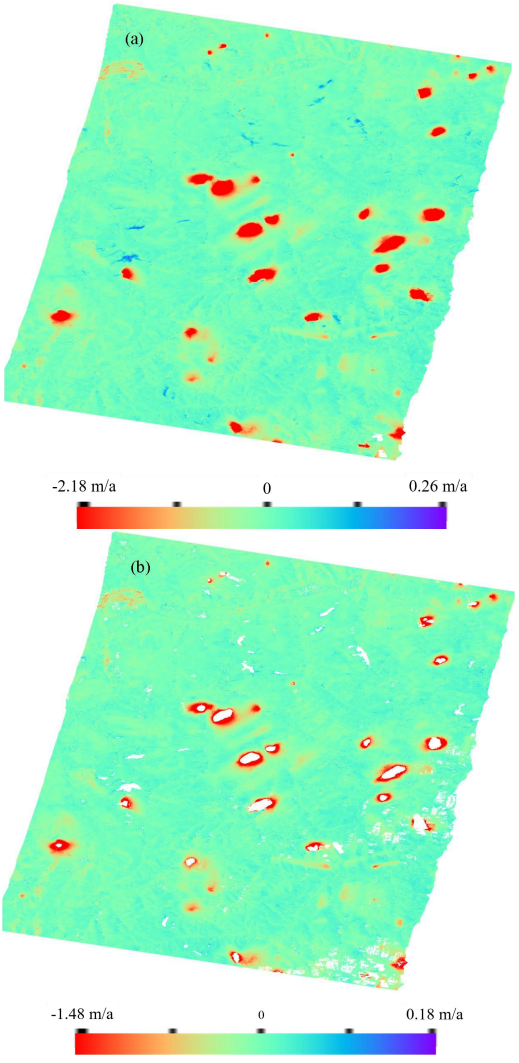

Figure 4. Stacking velocity results before and after refinement

4. DISCUSSION

Although DInSAR and stacking are both tools for monitoring surface deformation, their working principles and application scenarios are different, so their deformation field results may vary. Changes between the two results can be divided into three categories, see Table 2 (Mirmazloumi et al., 2022).

The first class is deformation areas which exist in DInSAR results, but not in the stacking results. It is possible that area (a) may be a deformation field in the short term, but it has disappeared in the long-term results, which might indicate a slight settlement in the short term. This phenomenon may be due to mining activities during the DInSAR monitoring period, but the excavation was quickly stopped (Filipiak and Borkowski et al., 2020; Chen et al., 2012). During mining operations, the terrain and geological structure of the mining area may be damaged, resulting in deformation phenomena such as ground collapse and cracks (Li et al., 2021). These deformations usually stabilize or recover gradually within a period of time after the mining activities cease. It is important to note that the phenomenon of short-term deformation and long-term disappearance in mining areas does not necessarily mean that the safety risks of mining activities have been reduced. In the planning and management of mining areas, it is necessary to comprehensively consider various factors, including geological structure, mining activities, and external environment, to ensure the safety and sustainable development of mining activities. What’s more, we found that the noise of area (d) almost disappeared due to the advantages of stacking.

The second class is deformation areas which exist in stacking results, but not in the DInSAR results. Areas (o) and (p) appearing in stacking results did not show any deformation in the DInSAR results, indicating that the deformation occurred later than the DInSAR data and is still ongoing. This may be due to the slow process of deformation or the small degree of deformation, which results in no significant changes in short-term data. Long-term deformation may be caused by mining activities, which may take a longer time to cause significant deformation, making it difficult to observe significant changes in short-term data. In order to better monitor and evaluate deformation in mining areas, regular deformation measurements and data analysis are needed. By comparing data at different time points, it is possible to better understanding the process and regularity of deformation, and take corresponding measures to ensure the safety and sustainable development of mining activities.

The third class is both DInSAR and stacking have, but changed. These changes exhibit different characteristics and have different causes. First, area (b) and area (k) exhibit a significant drift and a slight drift respectively, maybe caused by excavation depth, excavation volume and excavation direction of mining activities. Second, in the short term, there was a settlement in area (g), but in the long run, it has been uplifted, and there are more than a dozen such situations in the figure. It is possible that the uplift is caused by the continuous accumulation of slag caused by mining. Third, the movement in area (h) and area (i) maybe caused by the extension of the mining direction towards the northeast and west of these areas, respectively. The reason may be that the terrain and geological structure within the mining area have undergone deformation and displacement due to mining activities, geological tectonic movements, or other external factors, resulting in the continuous expansion of the deformation area. What’s more, the deformation areas in (j), (m) and (n) have obviously increased, indicating that the deformation in these areas is continuously deepening over time because of mining. The continuous subsidence of the mining area may be caused by factors such as the disturbance and destruction of underground rock formations during mining. During mining, the formation and expansion of the mined-out area will disturb the underground rock formations, destroy the original mechanical balance, and cause the rock formations to move, deform, and break. As mining progresses, this movement and destruction gradually spreads to the surface, causing surface subsidence. Finally, the deformation in area (l) has decreased, suggesting that the mining area showed significant deformation and displacement in the short term, but the deformation gradually reduced over time. In the short term, mining activities may cause significant disturbance and damage to the terrain and geological structure of the mining area, resulting in an increase in surface displacement and deformation displacement. However, over time, the underground rock layers may gradually reach a new mechanical equilibrium state, and the deformation displacement may gradually decrease. In addition, some natural factors such as earthquakes and rainfall may also affect the deformation displacement of the mining area.

Method	Type 1	Type 2	Type 3	total
DInSAR(2×2)	3	0	57	60
Stacking	0	2	30	32

Table 2. Comparison of the deformation fields number detected by two different techniques

Compared with DInSAR, the noise of stacking is well suppressed, but the deformation field number decreased greatly. In the study area, DInSAR detected a total of 60 deformation fields, while stacking only detected 32. On one hand, this indicates that DInSAR has higher sensitivity in processing data and can more accurately detect short-term surface deformation. However, due to the influence of multiple factors on radar signals, such as atmospheric conditions and surface types, noise interference may occur, which affects the accuracy of DInSAR data processing. Stacking can significantly improve prediction accuracy, but due to the superposition of multi-scene data and multiple models, the computational load is relatively large, and the processing speed is slower. On the other hand, in terms of application scenarios, DInSAR is suitable for various scenarios, including building, road, and mountain deformation, providing important data support for urban planning, disaster warning, and geological research (Jia et al., 2020). It’s suitable for situations of high coherence and nonlinear deformation. In contrast, stacking is suitable for long-term and large-scale deformation monitoring, less requiring on coherence and image quality. It is widely used in monitoring earthquake, volcanoes, glaciers, and tectonic movement (Chen et al., 2020). In summary, DInSAR and stacking each have advantages and are suitable for different scenarios. It is possible to select the appropriate method according to the specific requirements to obtain more accurate deformation field information.

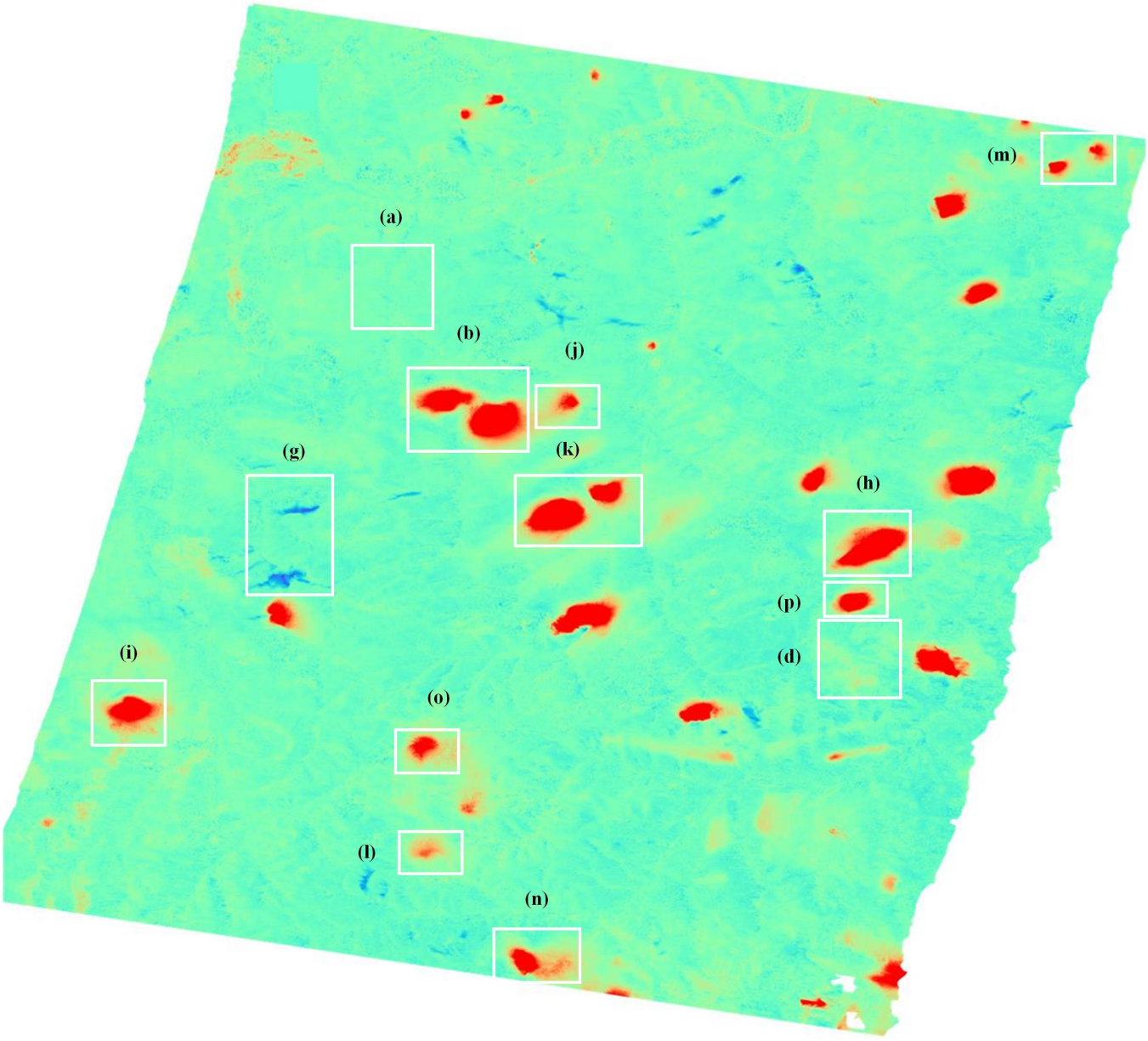

Figure 5. The changed deformation areas of stacking results compared with DInSAR results

5. CONCLUSIONS

In this paper, we tested the LandSAR software by assessing the DInSAR and stacking modules. We selected 21 LT-1 satellite data from 2022 to 2023 with a time span of 6 months, cut which into small images to make DInSAR and stacking processing. It is found that as the multi-look factor changing from 2×2 to 4×4, the coherence is getting higher, the noise is also reduced, but the null value of the deformation field increases with the increase of the multi-look factor due to the phase gradient after multi-look. Due to the decrease in image resolution caused by increasing the multi-look factor, there are 60 subsidence areas in the result with 2×2 multi-look factor, while only 47 subsidence areas in the result with 4×4 multi-look factor. Different from DInSAR, the processing results of stacking with the multi-look factor vary from 2×2 to 4×4 are very similar. Through adding a refinement method in the deformation rate calculation step, there is almost no obvious residual in the refined image but the values of most deformation fields are also eliminated as gross errors, resulting in a large ratio of null values in the results. Comparing with stacking, DInSAR can detect more deformation fields. DInSAR detected a total of 60 deformation fields, while stacking only detected 32. It proves that the deformation of coalfield is not linear. DInSAR has higher sensitivity in processing data and can more accurately detect short-term surface deformation, requiring high coherence and nonlinear deformation of images. Stacking requires less on coherence and image quality. Through supporting both DInSAR and Stacking algorithms, LandSAR can provide more accurate and reliable surface deformation monitoring and mineral resource exploration services, providing important decision support for natural resource management departments.

6. ACKNOWLEDGEMENT

This work was supported in part by National Key R&D Program of China (2021YFC3000405), the Young Scientists Fund of the National Natural Science Foundation of China (Grant NO. 42301160).

7. REFERENCES

T. Li, X. Tang, X. Zhou, X. Zhang, S. Li, and X. Gao, "Deformation Products of Lutan-1(LT-1) SAR Satellite Constellation for Geohazard Monitoring," presented at the IGARSS 2022, Kuala Lumpur, Malaysia, 2022.

J. Lu, X. Zhou, T. Li, X. Zhang, X. Zhang, T. Li, et al., " LandSAR Software Testing Method For LuTan-1 SAR Standard Product Generation In Natural Resource Monitoring " presented at the IET International Radar Conference, Chongqing, China, 2023.

T. Li, X. Tang, Q. Chen, Y. Liu, and X. Zhang, "Research on the Interferograms Selection Principles Using Gaofen-3 for DSM Production," in 2019 Asia-Pacific Conference on Synthetic Aperture Radar, Xiamen, China, 2019.

T. Li, T. Li, X. Zhou, J. Lu, X. Zhang, X. Zhang, et al., "An InSAR Processing Software Development and Management Method using Model-View-Controller Design Mode: LandSAR," in SAR in Big Data Era, Beijing, China, 2023.

J. Lu, X. Zhou, X. Zhang, X. Zhang, and L. Hu, "Big Data Oriented InSAR Software Testing Method For LandSAR Used In Chinese Satellite Lutan-1 Applications," presented at the SAR in Big Data Era, Beijing, China, 2023.

Y. Xu, T. Li, X. Tang, X. Zhang, H. Fan, and Y. Wang, "Research on the Applicability of DInSAR, Stacking-InSAR and SBAS-InSAR for Mining Region Subsidence Detection in the Datong Coalfield," Remote Sensing, vol. 14, p. 3314, 2022.

Y. Gao, S. Zhang, T. Li, Q. Chen, X. Zhang, and S. Li, "Refined Two-Stage Programming Approach of Phase Unwrapping for Multi-Baseline SAR Interferograms Using the Unscented Kalman Filter," Remote Sensing, vol. 11, p. 199, 2019.

Y. Gao, X. Tang, T. Li, Q. Chen, X. Zhang, S. Li, et al., "Bayesian Filtering Multi-Baseline Phase Unwrapping Method Based on a Two-Stage Programming Approach," Applied Sciences, vol. 10, p. 3139, 2020.

H. Johnsen, L. Lauknes, and T. Guneriussen, "Geocoding of fast-delivery ERS-l SAR image mode product using DEM data," International Journal of Remote Sensing, vol. 16, pp. 1957-1968, 2007.

Y. Xiang, F. Wang, and H. You, "An Automatic and Novel SAR Image Registration Algorithm: A Case Study of the Chinese GF-3 Satellite," Sensors (Basel), vol. 18, Feb 24 2018.

Y. Eshqi Molan, J.-W. Kim, Z. Lu, and P. Agram, "L-Band Temporal Coherence Assessment and Modeling Using Amplitude and Snow Depth over Interior Alaska," Remote Sensing, vol. 10, p. 150, 2018.

"Linear and non-linear long-term terrain deformation with DInSAR (CPT: Coherent Pixels Technique)," in Proceedings of the FRINGE workshop 2003, Frascatti, Italy, 2003, p. 21.1.

Z. Rui, X. Wei, L. Guoxiang, W. Xiaowen, M. Wenfei, F. Yin, et al., "Interferometric coherence and seasonal deformation characteristics analysis of saline soil based on Sentinel-1 A time series imagery," Journal of Systems Engineering and Electronics, vol. 32, pp. 170-1283, 2021.

L. Zhang, K. Dai, J. Deng, D. Ge, R. Liang, W. Li, et al., "Identifying Potential Landslides by Stacking-InSAR in Southwestern China and Its Performance Comparison with SBAS-InSAR," Remote Sensing, vol. 13, p. 3662, 2021.

K. Zhang, L. Ge, X. Li, and A. H.-M. Ng, "A robust regression-based linear model adjustment method for SAR interferogram stacking techniques," International Journal of Remote Sensing, vol. 34, pp. 5651-5665, 2013.

L. Zhu, H. Gong, P. Teatini, X. Li, R. Wang, B. Chen, et al., "Land Subsidence due to groundwater withdrawal in the northern Beijing plain, China," Engineering Geology, 2015.

S. M. Mirmazloumi, Y. Wassie, J. A. Navarro, R. Palamà, V. Krishnakumar, A. Barra, et al., "Classification of ground deformation using sentinel-1 persistent scatterer interferometry time series," GIScience & Remote Sensing, vol. 59, pp. 374-392, 2022.

K. Pawluszek-Filipiak and A. Borkowski, "Integration of DInSAR and SBAS Techniques to Determine Mining-Related Deformations Using Sentinel-1 Data: The Case Study of Rydułtowy Mine in Poland," Remote Sensing, vol. 12, p. 242, 2020.

F. Chen, H. Lin, Y. Zhang, and Z. Lu, "Ground subsidence geo-hazards induced by rapid urbanization: implications from InSAR observation and geological analysis," Nat. Hazards Earth Syst. Sci., vol. 12, pp. 935-942, 2012.

T. Li, "Lu Tan-1(LT-1)-The First Chinese L-Band Differential Interferometric SAR Satellites for Terrain and Subsidence Monitoring," in The 28th International Conference on Geoinformatics (Geoinformatics 2021 - CPGIS Annual Conference), Jiangxi, China, 2021.

H. Jia, Y. Wang, D. Ge, Y. Deng, and R. Wang, "Improved offset tracking for predisaster deformation monitoring of the 2018 Jinsha River landslide (Tibet, China)," Remote Sensing of Environment, vol. 247, p. 111899, 2020.

X. Chen, J. Peng, M. Motagh, Y. Zheng, M. Shi, H. Yang, et al., "Co-seismic deformation of the 2017 M s 7.0 Jiuzhaigou Earthquake observed with GaoFen-3 interferometry," International Journal of Remote Sensing, vol. 41, pp. 6618-6634, 2020.